Structure and photoluminescence features of nanocrystalline Si/SiO$_2$ films produced by plasma chemical vapor deposition and post-treatment

Xiaochun Wu,[a] Ch. Ossadnik, Ch. Eggs, and S. Veprek
Institute for Chemistry of Inorganic Materials, Technical University of Munich, Lichtenbergstrasse 4, D-85747 Garching, Germany

F. Phillipp
Max-Planck Institut fuer Metallforschung, Heisenbergstrasse 1, 70569 Stuttgart, Germany

Experimental results of the visible photoluminescence (PL) from nanocrystalline Si (nc-Si) embedded in a SiO$_2$ matrix, prepared by plasma Chemical vapor deposition and a subsequent post-treatment, are reported here. Scanning electron microscopy, transmission electron microscopy, x-ray diffraction, and Fourier transform infrared are used to characterize the morphology, crystallite size, and the composition and structure of nc-Si/SiO$_2$ films. The visible PL can be finely tuned from 1.3 to 1.75 eV by changing annealing time and temperature. The effect of high temperature (870 °C) forming gas (FG) annealing on the visible PL can be divided into three stages. In the first stage, the visible PL blueshifts from 1.3 to 1.55 eV, and the PL intensity increases. In the second stage, the peak energy shows a small shift, and the PL intensity continues increasing. In the last stage, the peak energy blueshifts to ~1.75 eV, but the PL intensity decreases. The visible PL shows a maximum intensity around 1.5 ± 0.05 eV. For a PL obtained after a high temperature anneal, a subsequent low temperature FG annealing (400 °C) will lead to a redshift of peak energy and an increase in PL intensity. In particular, for a PL around 1.75 eV, a kinetic oscillation of the spectral shift and the PL intensity has been observed upon this annealing. Detailed analysis indicates that the most probable candidates for the visible PL are two oxygen thermal donor-like defect states (TDs) (Si-NL8 and Si-NL10) generated during annealing. The effect of annealing temperature and time on the spectral change and the kinetic oscillation of the spectral change can be explained by the formation and decay kinetics of these two oxygen TDs-like defect states. On the one hand, these experimental results verified the Si–O bond related origin for the visible PL in this system; on the other hand, they also pointed out that apart from the common features of Si–O related visible PL, the detailed configuration and composition of this PL center by different synthesis methods may be different and possess some features of their own. © *2002 American Vacuum Society.* [DOI: 10.1116/1.1490389]

I. INTRODUCTION

Following the report of Canham about strong visible photoluminescence (PL) from porous silicon (PS),[1] much effort has been directed toward the understanding of the PL mechanism in order to develop the applications of Si-based devices in optoelectronics, displays, and sensors. Up to now, two models have been suggested for the source of the PL.[2,3] One model is a pure quantum size effect, i.e., the luminescence resulting from the radiative recombination of quantum-confined electrons and holes in PS.[4–7] A competing model for the source of the luminescence is surface-related defect structures, such as siloxene,[8] polysilanes,[9] SiH$_2$,[10] Si band-tail states,[11] interfacial oxide-related defect centers,[12] non-bridging oxygen hole centers (NBOHCs),[13] and oxyhydride-like emitters.[14] After 10 yr of research, a consensus about the origin of visible PL has been reached.[15–18] Either PS itself or the Si–O surface state can be the source of the visible PL, depending on the size of PS and on the interfacial chemical environment. A detailed mechanism was recently described by Wolkin *et al.*[15]

The most common method of fabricating PS films is an-

odic etching of a Si wafer in solutions containing HF and nonbiased chemical etching in HF/HNO$_3$ conditions. The resulting PL features depend on the etching conditions.[19] Typically, a broad, featureless emission is observed at room temperature centered at 550–800 nm with 200 nm full width at half maximum.[20] Since nanometer-sized Si structures in PS were believed to play an important role in the visible PL of PS, nc-Si particles produced by various dry chemical techniques have also been studied in order to understand the PL mechanism.[21–25] Si nanocrystallites produced by using these dry chemical techniques exhibit visible PL as well. In addition, solvent effects and complex electrochemical process are avoided in these dry chemical techniques. Although the systematic blueshift of the visible PL with the decrease of crystallite size in PS has rarely been mentioned,[26,27] it has been observed in nc-Si/SiO$_2$ films produced by some dry chemical methods due to the easy control of nanocrystalline (nc)-Si size.[28–30] The majority of the researchers ascribe this to the quantum size effect (QSE) since the blueshift of the visible PL is accompanied by a decrease in crystallite size due to oxidation treatment.

The red PL around 1.5 eV in nc-Si/SiO$_2$ films, produced by plasma chemical vapor deposition (CVD) and the subse-

---

quent post-treatment, has been reported in detail before.[31] It shows similar PL behavior to PS. Defect studies using the electron spin resonance (ESR) technique in this system afterward showed the correlation of the integrated PL intensity with the concentration of oxygen thermal donors (TDs)-related defect states, indicating that this kind of oxygen-related defect was responsible for the observed red PL.[32] Recently, we further extended our investigations to the effects of annealing temperature, atmosphere, and time on the spectral change of the visible PL between 1.5 and 1.75 eV.[33] It was found there that the spectral change (the spectral shift and the PL intensity) showed a strong and systematic dependence on annealing conditions and that the PL was actually composed of two PL centers.

In this article, apart from adding new *experimental results* of the visible PL, we will give a detailed description of the source and the spectral shift of the visible PL in this system. Scanning electron microscopy (SEM), transmission electron microscopy (TEM), x-ray diffraction (XRD), and Fourier transform infrared (FTIR) are used to characterize the morphology, crystallite size, and the composition and structure of nc-Si/SiO$_2$ films. The experimental results can be summarized as follows: (1) the visible PL can be finely tuned from 1.3 to 1.75 eV by a careful control of annealing time and temperature. (2) According to the observed PL features, the effect of high temperature (870 °C) forming gas (FG) annealing can be divided into three stages. In the first stage, the visible PL blueshifts from 1.3 to 1.55 eV, and the PL intensity increases. In the second stage, the peak energy shows a small shift, and the PL intensity continues to increase. In the last stage, the peak energy blueshifts to ~1.75 eV, but the PL intensity decreases. The visible PL shows a maximum intensity around 1.5±0.05 eV. (3) For a PL obtained after a high temperature anneal, a subsequent low temperature FG annealing (400 °C) will lead to a redshift of peak energy and an increase in PL intensity. In particular, a kinetic oscillation of spectral shift and PL intensity in the third stage has been observed upon this annealing. In agreement with our previous results,[31–33] these experimental results can be explained by the formation and decay kinetics of oxygen TD-like defect states. In addition, the relation between the nc-Si and oxygen TD-like defect states is also discussed. Finally, the structure and PL features of nc-Si/SiO$_2$ films have been compared with those of oxygen-terminated PS.

II. EXPERIMENT

A. Synthesis of nc-Si/SiO$_2$ films by plasma CVD and post-treatment

The synthesis consisted of the following four steps:

Step 1: The growth of an amorphous silicon film by plasma CVD. The film was further annealed under 0.03 mbar of hydrogen flow at 660 °C to decrease the amount of hydrogen in the film.

Step 2: The preoxidation of the amorphous silicon film in a resistance-heating oven under a flow of pure oxygen at 350 °C.

TABLE I. Weight film thickness, preoxidation time, and oxidation time.

Sample	Film thickness (μm)	Preoxidation time (350°)	Oxidation time (870°)
A	4	1 h	—
B	3	2 h	—
C	5.8	72 h 20 min	1 min
D	2.8	0.5 h	—

Step 3: The oxidation of the preoxidized film at 870 °C in pure oxygen. High temperatures lead to the crystallization of the amorphous films. Oxygen atmosphere leads to further oxidation of the film. Step 3 can be merged with Step 4 since the film has already adsorbed enough oxygen in step 2.

Step 4: Heating in a FG (95% nitrogen and 5% hydrogen) at 870 °C for a chosen time.

The advantages of this technique are: (1) Similar to other dry chemical techniques, it is compatible with modern microelectronic technology. (2) The synthesis conditions are easy to control. Thus, the changes of the visible PL can be finely tuned and show a good reproducibility.

Here, the visible PL from four samples is shown. Weight film thickness, preoxidation time, and oxidation time are given in Table I. FG annealing conditions are given in the corresponding figures.

B. Structural characterization and spectroscopy

The surface morphology was observed with a SEM (Hitachi S-800). A TEM (JEOL 4000FX) was used to obtain the size of nc-Si and its distribution. One piece of nc-Si/SiO$_2$ film was scratched off the wafer and ultrasonically dissolved in ethanol. Grids were prepared by depositing the obtained colloidal solution onto a 400 mesh copper grid and dried in air. XRD (Siemens D-5000 powder diffractometer) was used to obtain the average particle size and the fraction of nc-Si in the film. The FTIR spectrometer was a Perkin Elmer FTIR 1760X. All FTIR spectra were recorded at 4 cm^{-1} resolution and averaged using 40 scans. Laser PL measurements were done by illuminating the sample using the 325 nm line of a He–Cd laser (Omnichrome series 56) with a maximum pump power density of 0.4 W/cm^2 (100% laser intensity). Except for the laser intensity dependence experiment, all other PL spectra were measured at 100% laser intensity. The obtained PL signals were collected and focused into a monochromator (Spex Model 1681B) and detected by a Si diode in the lock-in mode. A PC controlled data collection. A tungsten standard lamp was used to calibrate of the spectral sensitivity of whole measuring system. PL excitation spectra (PLE) were measured using Perkin Elmer LS 50B fluorometer. All measurements were done at room temperature.

III. RESULTS

A. Structural characterization of nc-Si/SiO$_2$ films

1. XRD characterization

Figure 1 shows the effect of FG annealing time on the XRD patterns for sample A. It is a representative evolution
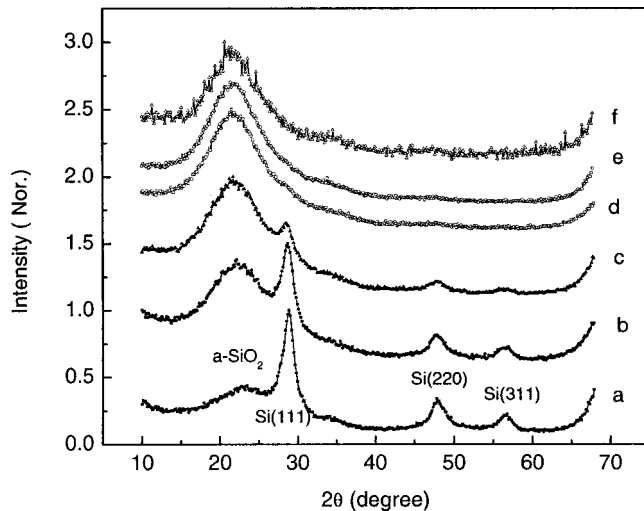
FIG. 1. Evolution of XRD diagrams of sample A upon 870 °C FG annealing: (a) 24 min, (b) 2 h 36 min, (c) 3 h 36 min, (d) 5 h 36 min, (e) 7 h, and (f) 7 h 30 min.

FIG. 2. SEM topographic image of nc-Si/SiO$_2$ film after 15 min FG annealing at 870 °C.

of XRD diagrams of nc-Si/SiO$_2$ films upon high temperature FG annealing. The appearance of three main diffraction peaks of Si (111), Si (220), and Si (311) in Fig. 1(a) indicates the existence of Si nanocrystallites. The broad diffraction peak around 22° belongs to amorphous SiO$_2$. Therefore, the film consists of nc-Si and amorphous SiO$_2$. With increasing FG time [Figs. 1(b)–1(f)], the particle size and amount of nc-Si in the film decreases. The average particle size was obtained from the measured integral half width of the Bragg reflections using the Scherrer formula. It decreases from 4 nm of Fig. 1(a) to below 2 nm of Fig. 1(d). The relative amount of nc-Si in the films has been determined from the XRD pattern.[34,35] It decreases from over 40% of Fig. 1(a) to about 6% of Fig. 1(d). Due to too weak signals for nc-Si in Figs. 1(e) and 1(f), we did not evaluate the size and amount of nc-Si for these two annealing times.

2. SEM and TEM measurements

Figure 2 is a SEM topographic image of one sample, which was annealed at 870 °C for 15 min. The obtained nc-Si/SiO$_2$ film is a porous film. Figure 3 is the TEM images of the same sample. The bright field image [Fig. 3 (a)] shows many isolated particles with an average size around 10 nm. The corresponding dark field image [Fig. 3 (b)] shows many isolated particles with a smaller average size around 5 nm. Since our film is a composite material and is composed of amorphous SiO$_2$ and nc-Si, the difference between the bright field image and the dark field image indicates that nc-Si particles are covered with an amorphous SiO$_2$ layer. Because dark field image is more sensitive to the crystalline phase, the size of nc-Si obtained from the dark field image therefore is more accurate in our system. It is a little larger than the average particle size (4.3 nm) calculated from XRD patterns [not shown here, similar to Fig. 1(a)]. From the dark field image, it can be seen that the crystallites are distributed in size. High resolution TEM image [Fig. 3(c)] exhibits the lat-
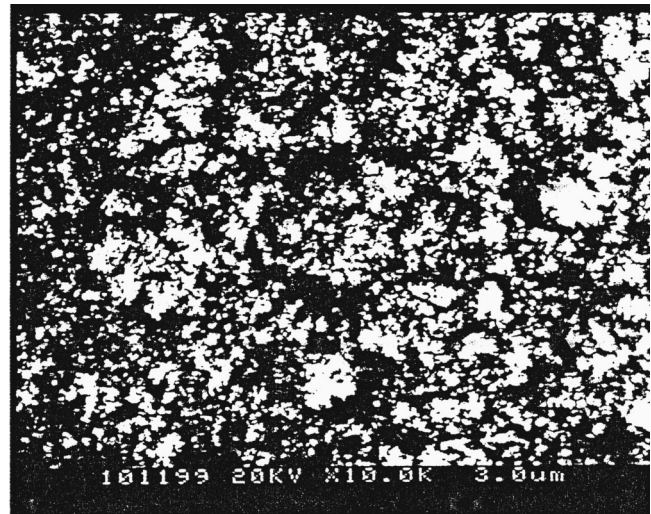
tice fringes corresponding to the (111)-lattice planes of Si. However, due to the little amount of nc-Si in the films, we did not succeed in obtaining the nc-Si size for samples with longer FG time that show a strong visible PL around 1.5 eV. Therefore, the sizes of nc-Si for PL samples were obtained from XRD data.
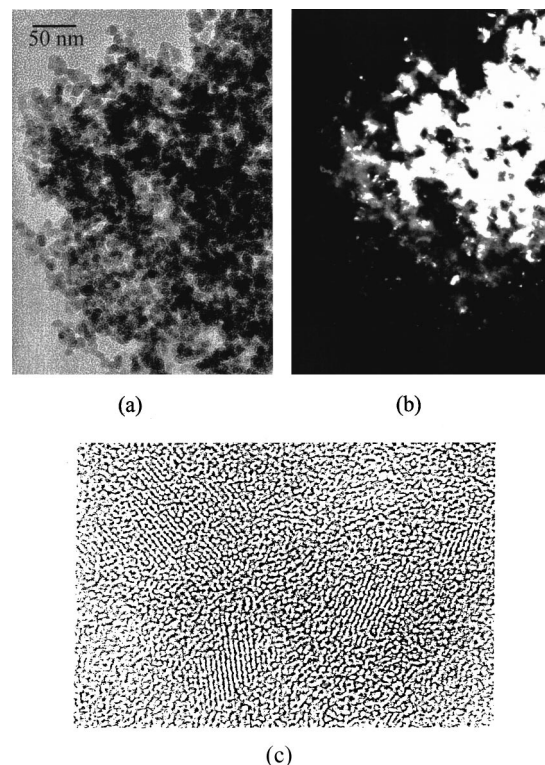

FIG. 3. TEM images for the sample of Fig. 2: (a) bright field image, (b) dark field image, and (c) high resolution lattice image.
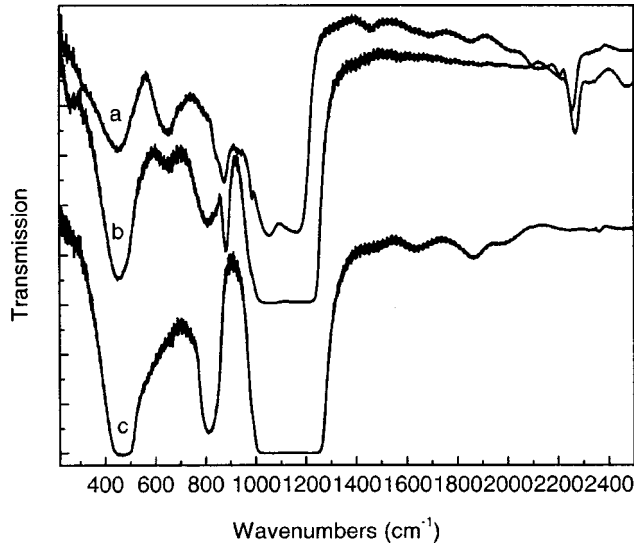
FIG. 4. Evolution of FTIR absorption spectra at different steps of post-treatment process: (a) before preoxidation, (b) after preoxidation, and (c) after 1 h of FG annealing at 870 °C.

3. FTIR absorption spectra

Figure 4 shows a typical change of FTIR absorption spectra during the post-treatment process. The assignment of the main vibrational features is as follows:[36–38] the double-peak structure between 900 and 1200 cm⁻¹ is the Si–O–Si stretching vibration; 810 cm⁻¹ is Si–O–Si bending vibration, and 460 cm⁻¹ is a Si–O–Si rocking vibration; the 650 cm⁻¹ band is composed of SiH and SiH₂ bending vibrations; 870 cm⁻¹ is SiH₂ scissors vibration; and 2250 cm⁻¹ is H-SiOx stretching vibration. Figure 4(a) is the FTIR spectrum of one film before preoxidation. Since the film is porous and adsorbs oxygen easily from air, the vibrational bands related to Si–O bonds are also observed before the preoxidation. After preoxidation, the vibration absorbance intensities related to Si–O bonds increase, whereas those of Si–H bonds decrease due to the substitution by Si–O bonds [Fig. 4(b)]. After 1 h of FG annealing at 870 °C, the vibrational bands related to Si–H bonds further decrease [Fig. 4(c)]. More FG annealing leads to the further enhancement of Si–O vibration absorbance modes.

From SEM, TEM, XRD, and FTIR characterizations, it can be seen that the prepared nc-Si/SiO₂ films are porous films and are composed of nc-Si and amorphous SiO₂. Upon FG annealing, the size and amount of nc-Si in the film decreases due to the oxidation process.

B. Visible PL features of nc-Si/SiO₂ films

1. Visible PL features upon high temperature FG annealing

The red PL centered around 1.5 eV has been discussed in detail in this system before.[31] We found out here that by a careful control of annealing times upon high temperature FG annealing, the visible PL can be finely tuned from 1.3 to 1.75 eV. The variation of this visible PL can be divided into three stages. Figure 5 is one example, which exhibits the evolution
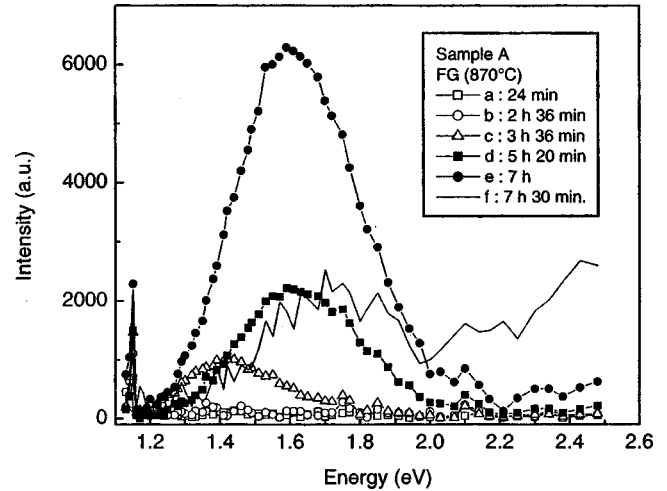

FIG. 5. Evolution of visible PL spectra with increasing time upon 870 °C FG annealing for sample A: (a) 24 min, (b) 2 h 36 min, (c) 3 h 36 min, (d) 5 h 36 min, (e) 7 h, and (f) 7 h 30 min.

of visible PL spectra upon increasing annealing times for sample A. The corresponding change in XRD patterns is shown in Fig. 1. In the first stage, the visible PL blueshifts from 1.3 to 1.6 eV [Figs. 5(c)–5(d)], and the PL intensity increases. In the second stage, the peak energy shows a small shift, and the PL intensity continues increasing [Figs. 5(d)–5(e)]. In the last stage, the peak energy blueshifts from 1.6 to ~1.75 eV [Figs. 5(e)–5(f)], but the PL intensity decreases. The visible PL shows a maximum intensity around 1.6 eV for this sample.

2. Blueshift of the visible PL in the first stage

Figures 6(a)–6(c) shows the blueshift of the visible PL for sample B in the first stage. With more FG annealing, the visible PL gradually blueshifts, and its PL intensity increases. At the same time, the size and amount of nc-Si decreases upon FG annealing (Fig. 6 inset). Similar to the observations
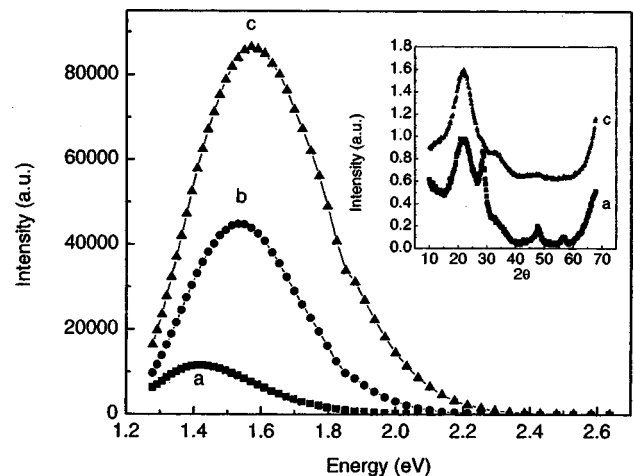

FIG. 6. Blueshift of visible PL of sample B in the first stage upon 870 °C FG annealing: (a) 2 h 20 min, (b) 6 h 20 min, and (c) 9h 20 min. (Inset) XRD diagrams after 2 h 20 min and 9 h 20 min annealing.
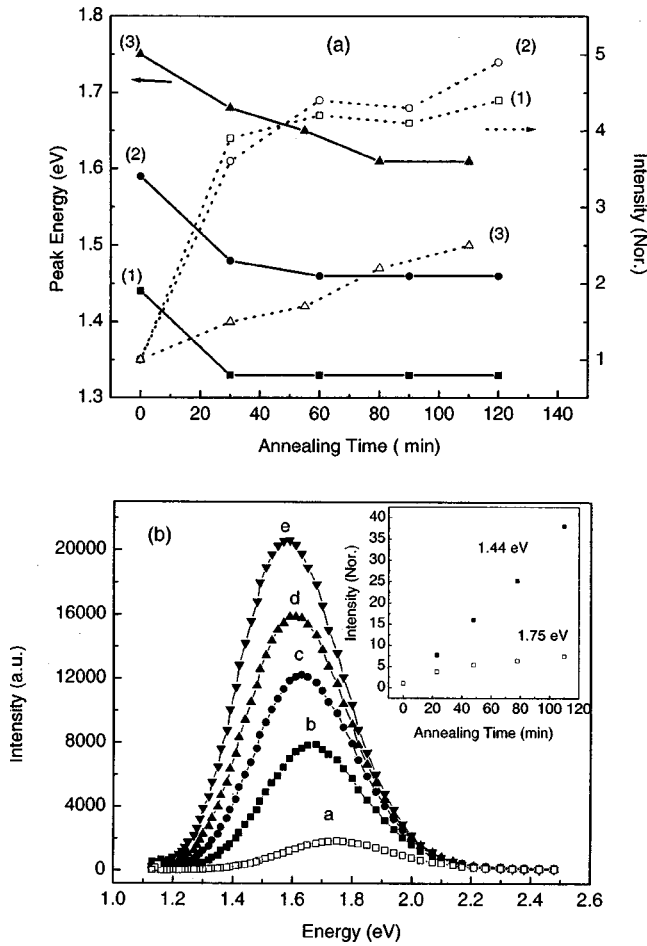
FIG. 7. (a) Evolution of peak energy (left side) and PL intensity (right side) vs annealing times upon 400 °C annealing for three samples with different initial peak energies: (1) 1.44 eV, (2) 1.59 eV, and (3) 1.75 eV. The lines are guides to the eye. (b) Evolution of visible PL spectra upon FG annealing at 400 °C.

FIG. 8. Spectral shift of the visible PL on laser intensity for sample B (a) and for sample C (b) with I/I_0 (%): (a) 100, (b) 30, (c) 17.4, (d) 10, (e) 1.74, and (f) 0.525. (I_0 is 100% laser power.) (Inset) Dependence of the integral PL intensity on the excitation power (dots) and linear fitting (lines).

by other researchers mentioned above,[28–30] the systematic blueshift of the visible PL with the decrease of nc-Si size is also observed here. Sample B after 2 h 20 min of FG annealing has 3.5 nm of average particle size and about 36% of nc-Si amount in the film. This sample after 9 h 20 min of FG annealing has an average particle size of less than 2 nm and the nc-Si amount below 4%. According to the theoretical calculation,[39] 3.5 and 2 nm nc-Si particles should have band gaps of around 2 and 2.8 eV, respectively. The PL peak energy shifts from 1.41 eV of Fig. 6(a) to 1.57 eV of Fig. 6(c). The peak shift is below 0.2 eV, i.e., much smaller than the blueshift of the nc-Si band gap with the decrease of crystallite dimension based on the theoretical calculations.[40–43]

3. Redshift of the visible PL upon FG annealing at 400 °C

It was found that the visible PL, obtained after a high temperature anneal, exhibited a redshift in peak energy and an increase in PL intensity upon a subsequent low temperature annealing. Figure 7(a) displays the spectral shift and the PL intensity variation versus annealing time for three
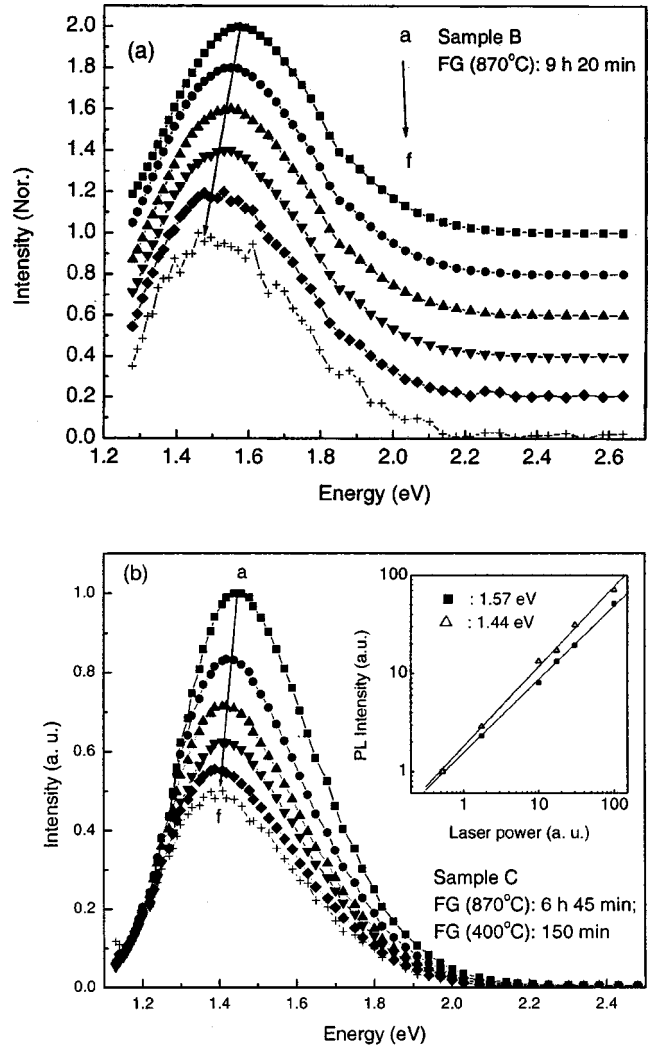
samples with different initial peak energies upon a further 400 °C FG anneal. After 120 min of annealing, the visible PL in all three samples demonstrates at least 0.1 eV of redshift in peak energy and a different magnitude of increase in PL intensity. XRD and FTIR measurements show no observable change upon this annealing procedure. Therefore, this redshift has no direct correlation with the variation of crystallite size. Figure 7(b) shows the evolution of visible PL spectra with increasing annealing time for one sample. The peak energy redshifts from 1.75 to 1.59 eV after 110 min annealing. The increased rate of the PL intensity at the lower energy side (1.44 eV) is much larger than that at the higher energy side (1.75 eV) [Fig. 7(b) inset].

4. Dependence of the visible PL on laser intensity

Since the nc-Si/SiO$_2$ films show a strong visible PL in the second stage, the dependence of this PL on laser intensity by decreasing laser intensity is further measured. Figure 8(a) is
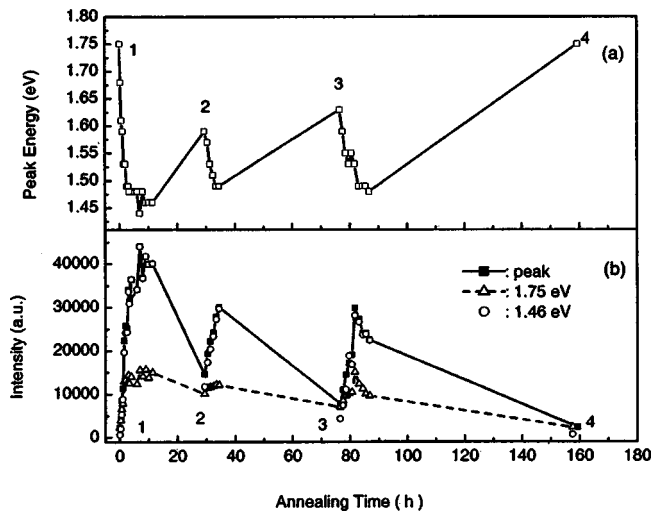
FIG. 9. Spectral shift (a) and PL intensities (b) vs accumulation annealing times upon a 400 °C FG annealing process for sample D: a demonstration of spectral oscillatory behavior.

for sample B, which emits PL with a peak energy of 1.57 eV. Figure 8(b) is for sample C, whose peak energy has red-shifted from 1.59 to 1.44 eV after a further 400 °C FG annealing. The curves are normalized and shifted for comparison. Decreasing laser intensity, both samples show the redshift of the peak energy. It redshifts from 1.57 to 1.49 eV for sample B and from 1.44 to 1.39 eV for sample C. Figure 8(b) (inset) shows the dependence of integral PL intensities I_{PL} on excitation powers P and their approximation by a power-law function ($I_{PL} \sim P^\gamma$). For the convenience of comparison, the PL intensities for both samples are normalized by their PL intensities at 0.525% of the maximum excitation power. The dependence for both samples deviates from linear relationship ($\gamma = 1$), with $\gamma = 0.75$ for sample B and $\gamma = 0.82$ for sample C.

5. Spectral oscillatory behavior of the visible PL

An interesting spectral oscillatory behavior in the third stage (between 1.75 and 1.5 eV) has been observed upon 400 °C FG annealing.[44] For a PL around 1.75 eV, at shorter annealing times, it gradually redshifts to ~1.5 eV, accompanied by an increase in intensity. At longer annealing times, it blueshifts, accompanied by a decrease in intensity. One example is shown for sample D in Fig. 9. It clearly demonstrates that both the spectral shift and the intensity variation versus accumulation annealing times exhibit temporal oscillatory behavior. Each oscillation is composed of two time segments, i.e., a shorter time segment with a redshift of the peak energy and an increase in intensity and a longer time segment with a blueshift of the peak energy and a decrease in intensity.

6. Source of photoexcitation process PLE spectra

In order to obtain some information about the light excitation process, the PLE spectra of nc-Si/SiO$_2$ films have been measured. The PLE spectra have been corrected by the

fluorometer. Figure 10(a) shows laser PL spectra of sample C before (referred to as C1 here) and after (referred to as C2 here) a 400 °C FG anneal. After 150 min annealing at 400 °C, the PL shifts from 1.59 to 1.44 eV, a 0.15 eV red-shift, and the PL intensity obviously increases. Arrows in Fig. 10(a) indicate the positions of emission wavelengths of 720 and 830 nm. Figure 10(b) shows the PLE spectra for C2 at different emission wavelengths, with the normalized PLE spectra at emission wavelengths of 830 and 710 nm are shown in the inset. The feature around 390 nm is due to the instrument. The PL intensities show a gradual increase with the increase of excitation energy. This indicates that nc-Si still remains the features of an indirect band-gap semiconductor. In addition, PS normally shows monitoring-wavelength-dependent PLE spectra, which was considered as coming from the inhomogeneous structure of PS.[45–50] In our case this dependence is not obvious as shown in the Fig. 10(b) inset. Since at different PL emission wavelengths the PLE spectra have no obvious change, this indicates that in our case the effect of nc-Si size distribution is not a dominate factor to the spectral distribution of the PL. Figure 10(c) shows a comparison of PLE spectra for C1 and C2, with the normalized PLE spectra at emission wavelengths of 720 nm for C1 and 830 nm for C2 shown in the inset. Although the peak energy of PL spectra has a 0.15 eV shift between C1 and C2, their PLE spectra are nearly the same. This suggests that the redshift of the PL upon low temperature FG annealing is not due to the variation of nc-Si size.

IV. DISCUSSION

A. Source of the visible PL

Our previous studies showed that oxygen TD-like defect states were the most likely candidates for the visible PL in our system and that the visible PL is composed of two oxygen TD-like defect states with different thermal stability.[31–33] Here we further analyze the following two experimental results, which exclude the nc-Si itself as the source of the visible PL in our system.

For the QSE model, both the excitation and emission process comes from nc-Si itself. Therefore, a redshift of the PL should be accompanied by a similar redshift of the band gap due to the increase in nc-Si size. This effect will be exhibited more obviously in excitation spectra than in absorption spectra since only those nc-Si particles that contribute to the PL are counted in excitation spectra. Figure 10(c) shows the excitation spectra of 1.59 eV PL and those of 1.44 eV PL that were obtained after a further 150 min 400 °C annealing. If we assume that the PL around 1.59 eV is due to the smaller nc-Si particles and that the PL around 1.44 eV is due to the larger ones, according to the QSE model, the excitation spectra of the latter should show at least 0.15 eV redshift compared with those of the former. The experimental results, however, show no shift of excitation spectra [Fig. 10(c) inset]. They, on the contrary, support the surface state model, where the excitation and emission processes come from different entities. If we assume that the excitation process comes from the nc-Si itself while the PL comes from the
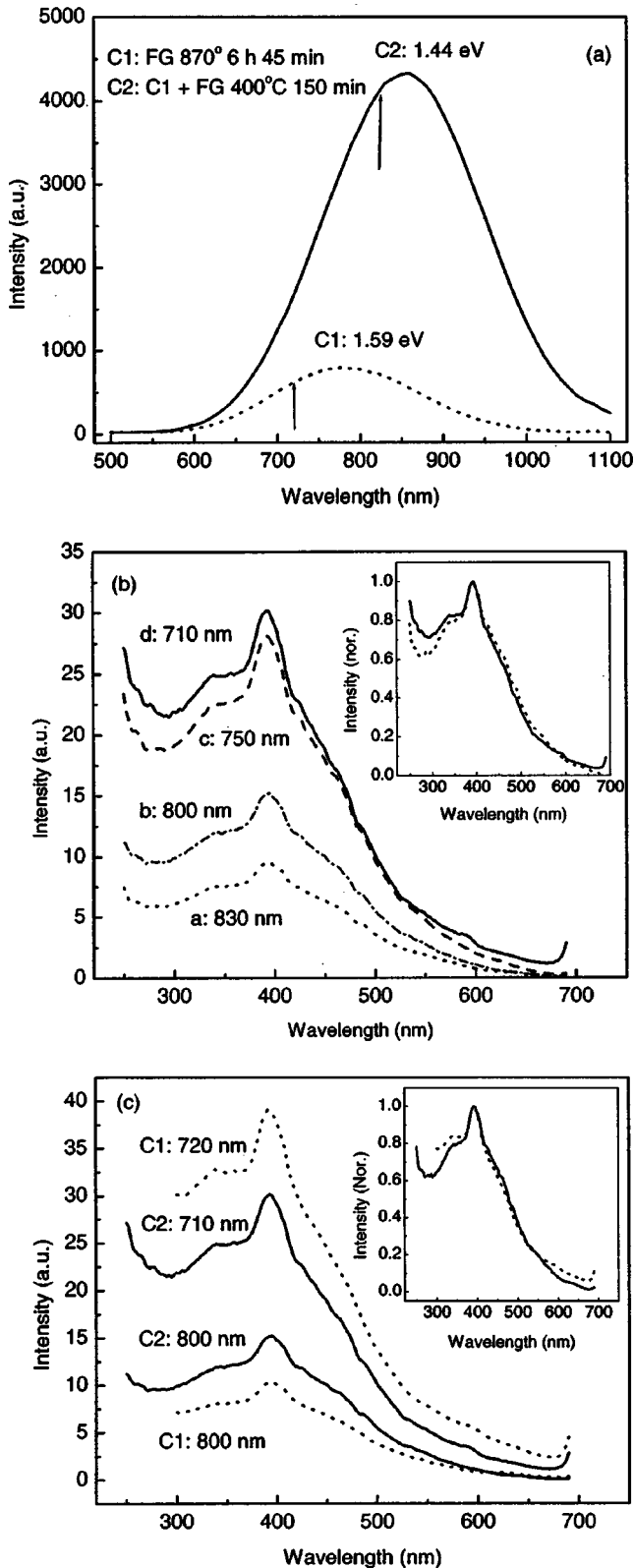
FIG. 10. (a) Laser PL spectra of sample C before (C1) and after (C2) 400 °C FG annealing. Arrows indicate the positions of emission wavelengths of 720 and 830 nm. (b) PLE spectra for C2 at different emission wavelengths, with the normalized PLE spectra at emission wavelengths of 830 and 710 nm shown in inset. (c) Comparison of PLE spectra for C1 and C2, with the normalized PLE spectra at emission wavelengths of 720 nm for C1 (dotted line) and 830 nm for C2 (solid line) shown in inset.

defect state energy levels within the band gap of nc-Si, then the change of PL energies has no necessary connection with the size of nc-Si.

The kinetic oscillatory behavior shown in Fig. 9(b) indicates that both the lower energy PL centers and the higher energy PL centers exhibit the oscillatory behavior. In addition, as shown in Fig. 9 points 1, 2, and 3, the regrowth of PL centers can be initiated at different peak energies. This indicates that the oscillatory behavior observed here is purely kinetic. This excludes the possibilities of the structural phase transition, by considering 1.5 eV PL as one structure of nc-Si and 1.75 eV PL as another structure of nc-Si, or the size variation of nc-Si itself as the source of the oscillation. This therefore rules out nc-Si itself as the source for the visible PL.

The assumption of two oxygen TD-like defect states can explain the visible PL in our system. Oxygen TDs widely exist in oxygen-enriched crystalline silicon under low temperature annealing ($<550 °C$).[51] From ESR measurement, mainly two signals (Si NL8 and Si NL10 centers) are related to oxygen TDs. The formation process of the Si NL8 center is normally faster than that of the Si NL10 center. The Si NL8 center is less stable at longer annealing times and at higher annealing temperatures compared with the Si-NL10 center.[52] The concentration of oxygen TDs in crystalline Si from ESR measurements upon low temperature annealing first increases with annealing times, then reaches a maximum, and finally decreases.[52] It can be seen from Fig. 9 for each oscillation that the intensity variation of the visible PL with annealing time shows the same trend with the concentration variation of oxygen TDs with annealing time. According to the variance in thermal stability of the two PL centers, the PL around 1.75 eV was ascribed mainly to the Si NL10-like defect state while the PL around 1.5 eV was ascribed to both Si NL8- and Si NL10-like defect states.[33] The Si NL8 center contributes to the lower energy side of the visible PL while the Si NL10 center contributes to the higher energy side.

In the first stage, due to the high temperature oxidation of nc-Si by adsorbed oxygen in the film, on one hand the size and the fraction of nc-Si in the film decrease [Figs. 1(a)–1(d)]; on the other hand, oxygen TDs form. During this stage, the color of the film changes from brown to gray, and the structure of nc-Si/SiO₂ films changes greatly. In the second stage, since the amount of residual oxygen in the film is small, the oxidation reaction is very slow [Figs. 1(d)–1(e)]. This stage corresponds to the continuing growth process of oxygen TDs before they reach their saturation concentrations, as shown in Figs. 5(d)–5(e). In this stage, we observe the strongest visible PL. The detailed peak energy of this strong PL is determined by the relative amount of these two TDs. In the third stage, the PL intensity obviously decreases. This is due mainly to the instability of oxygen TDs. Longer FG annealing will damage oxygen TDs. This will lead to a decrease in the PL intensity. Since the stability of the Si NL10 center is higher than that of the Si NL8 center and both centers contribute to the visible PL, after a certain time

the Si NL8 centers are completely damaged, while some Si NL10 centers still remain. These Si NL10 centers give a visible PL around 1.75 eV with a low intensity. Further annealing at high temperature will also lead to the complete damage of Si NL10 centers. This will result in the disappearance of the visible PL in this range and the appearance of a new PL around 2.8 eV, which has been discussed before.[31]

In our case, we did not find the PL from nc-Si itself although it can give PL. Due to the effective trap of photoinduced carriers to the oxygen TD-like defect states, the PL from nc-Si itself was quenched. This agrees with experimental results from oxygen-terminated PS and nc-Si formed via the implantation of Si$^+$ into SiO$_2$.[15,17,18]

B. Origin of blueshift upon high temperature FG annealing

Wolkin *et al.* have made a detailed investigation of the visible PL in PS.[15] They classified PS into hydrogen-terminated PS and oxygen-terminated PS. They found that for hydrogen-terminated PS, recombination is via the free excitons states for all sizes. The PL energy is equal to the free exciton band gap and follows the QSE model. For oxygen-passivated PS, depending on the size of the Si cluster, three recombination mechanisms are suggested. At the large size, recombination is via free excitons since the band gap is not wide enough to stabilize the Si=O surface state. At the medium size, recombination involves a trapped electron and a free hole. As the size decreases, the PL emission energy still increases, but not as fast as predicted by the QSE model, since the trapped electron state energy is size independent. At quite a small size, recombination is via trapped excitons (Si=O surface state). As the size decreases, the PLE remains constant (around 2 eV). In our case, the spectral shift from 1.3 to 1.75 eV can be divided into two ranges. The blueshift from 1.3 to 1.55 eV [Figs. 6(a)–6(c)] is similar to the case of medium size since the blueshift of the PL accompanies the decrease of the nc-Si size, but is smaller than the blueshift predicted by the QSE [Figs. 6(a)–6(c) inset]. The spectral change from 1.5 to 1.75 eV corresponds to the case of quite small size, i.e., recombination is via trapped excitons. However, in our case, the PL energy does not remain constant due to the coexistence of the two PL centers with different emission energies in one PL and to their variance in annealing temperature and time dependence.

In the first stage (from 1.3 to 1.55 eV), the explanation of spectral change is more complicated since the formation and decay of oxygen TDs and the oxidation of nc-Si take place concurrently, but have different kinetics. In addition, as discussed above, the visible PL is composed of two oxygen TDs. The change in the concentration ratio of these two oxygen TDs upon annealing time also contribute to the spectral shift. All these will lead to a complex dependence of spectral shift on the QSE. In the second and third stages, the size of nc-Si does not change due to the completion of oxidation reaction of nc-Si. Therefore, we can well explain the observed spectral changes between 1.5 and 1.75 eV using the formation and decay kinetics of oxygen TDs.

C. Spectral shift and intensity variation of the visible PL

The visible PL obtained after a high temperature anneal shows a redshift of the peak energy and an increase of the PL intensity upon a subsequent 400 °C anneal. This is due to the temperature dependence of the saturation concentrations of oxygen TDs.[53] The saturation concentrations of oxygen TDs at 400 °C are higher than those at higher annealing temperatures since oxygen TDs have a higher decay rate at higher temperatures. For a visible PL obtained after a higher temperature anneal, the subsequent lower temperature anneal will lead to the regrowth of oxygen TDs. As the growth rate of the Si NL8 center at lower temperature for shorter time is higher than that of Si NL 10 centers, this will lead to a larger increase in the concentration of Si NL8 centers compared with that of Si NL10 centers [see Fig. 7(b) inset]. Because Si NL8 centers contribute to the low energy side of the visible PL, this will lead to the redshift of the visible PL. Due to the increase in the total concentration of oxygen TDs, the PL intensity also correspondingly increases.

The laser-power dependence of spectral changes is also related to these two centers. The sublinear character indicates the saturation of PL intensities. This is due to the limited numbers of PL centers. The blueshift of the peak energy with laser intensity suggests that the Si NL8 center is a more effective trap center as compared to the Si NL10. With the increase of laser power, Si NL8 centers trend to saturate, and Si NL10 centers are more effectively populated. Since PL from Si NL10 centers is at the higher energy side of the visible PL, this will lead to the blueshift of the peak energy with the increase of laser power. As already known from above, low temperature annealing can effectively increase the concentrations of the two PL centers, with more increase in Si NL8 centers. Due to this increase in the total concentration of the PL centers, the saturation effect will decrease. The increase of γ from 0.75 of sample B to 0.82 of sample C verified this. Due to the larger increase of Si NL8 centers than that of Si NL10 centers, the degree of the blueshift with laser intensity should also decrease. This is also justified by sample C. The spectral blueshift of 0.05 eV in sample C is smaller than that of 0.08 eV in sample B.

Spectral oscillatory behavior between 1.75 and 1.5 eV can be interpreted by two oxygen TD models as well. The redshift from 1.75 to 1.5 eV corresponds to the growth process of oxygen TDs while the blueshift from 1.5 to 1.75 eV corresponds to the decay process of them. Oxygen TDs at 400 °C have a much faster growth rate compared with their decay rate. This can be seen from shorter annealing times required for the increase of the PL intensity and from longer annealing time required for the decrease of the PL intensity. We can explain the spectral shift and intensity variation upon annealing time as follows: Low temperature annealing first leads to the growth of oxygen TDs. Since the growth rate of Si NL8 centers are faster than that of Si NL10 centers, the increase in PL intensity at the lower energy side is larger than that at the higher energy side. This leads to a redshift of the peak energy, accompanied by an increase in PL intensity.
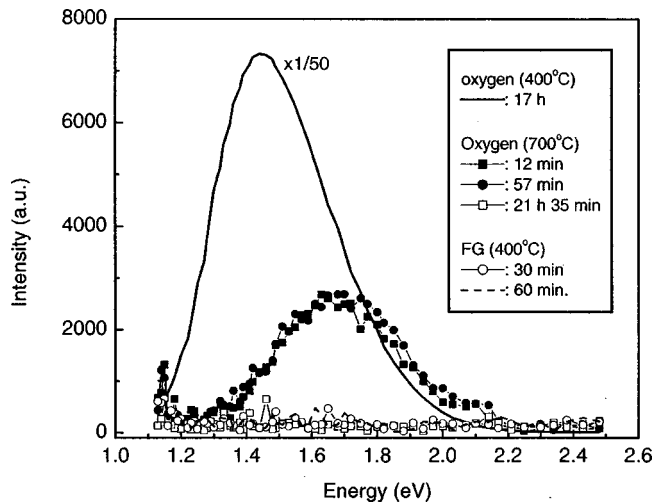
FIG. 11. Effect of annealing temperature and atmosphere on visible PL spectra: the dependence of the visible PL on nc-Si.

After reaching their maximum concentrations, oxygen TDs begin to decay. Since the decay rate of Si NL8 centers is faster than that of Si NL10 centers, the decrease of PL intensity at the lower energy side is larger than that at the higher energy side. This leads to a blueshift of peak energy, accompanied by a decrease in intensity. In one word, the variance in the growth and decay kinetics of Si NL8 and Si NL10 centers leads to the observed spectral changes. Thus, the shorter time segment corresponds to the growth process of oxygen TDs while the longer time segment corresponds to the decay process of oxygen TDs.

Apart from the intensity at the peak energy, the intensities at 1.75 and 1.46 eV versus annealing time are also displayed in Fig. 9(b). Si NL8 centers and Si NL10 centers exhibit similar growth and decay processes. Both the growth rate and the decay rate of Si NL8 centers are faster than those of Si NL10 centers. Since this oscillatory behavior is purely kinetic, it means that the oscillatory elements are metastable species. This agrees with the intermediate-state characters of oxygen TDs. An autocatalysis process drives the regrowth of oxygen TD-like defect states during their decay process and gives rise to this spectral oscillatory behavior. At present, the source for this autocalysis is however unclear.

D. Relation of the visible PL to nc-Si

Since oxygen TDs are observed only in bulk crystalline Si, the existence of nc-Si is a prerequisite for the formation of oxygen TDs. The dependence of oxygen TDs on nc-Si is shown in Fig. 11. Annealing at 700 °C under oxygen atmosphere has a great influence on the visible PL. After a short time anneal, the PL blueshifts from 1.44 to 1.68 eV, and the PL intensity decreases greatly. The asymmetric PL around 1.44 eV also becomes a more symmetric PL around 1.68 eV. These indicate that both the higher energy PL centers and the lower energy PL centers are damaged. Due to the higher decay rate of the lower energy PL, the higher energy PL centers dominate the visible PL. This leads to a more sym-

metric visible PL. After a long time annealing, nc-Si particles were totally oxidized, and the visible PL disappeared. A subsequent FG annealing at 400 °C cannot lead to the reappearance of the visible PL. This agrees with the observation that oxygen TDs have only been observed in crystalline Si in bulk. On the other hand, the existence of nc-Si is not a sufficient condition for the appearance of the visible PL. The sample whose TEM image [Fig. 3(b)] demonstrated the existence of many isolated, several nanometer-sized Si particles gives no visible PL. The reason is that oxygen TDs have not formed due to the very short FG annealing time (15 min at 870 °C). The PL normally appears after 2 h of 870 °C FG annealing, although there exists certain time differences among different samples. Therefore, the existence of nc-Si is a prerequisite, but not a sufficient condition for the visible PL.

E. Relation of the visible PL in nc-Si to the visible PL in oxygen-terminated PS

As stated in Sec. I, Si–O related surface species have been recognized as one source of the visible PL in PS and nc-Si related materials.[8,12–14] However, the understanding of the structure and composition of Si–O related surface species is still in the early stage. For example, the visible PLs with peak energies from 1.5 to 2.1 eV have been ascribed to Si–O related surface species without detailed structure information. According to theoretical calculation, Wolkin *et al.* suggested that a special Si=O surface state is responsible for the 2.1 eV visible PL in very small, oxygen terminated PS.[15] However, this Si=O bond has not been verified experimentally up to now. Based on time-resolved FTIR studies, Wang *et al.* established the correlation between visible PL and Si–O bond related surface species in their aged PS samples.[18] Among various Si–O related species, NBOHCs are probably the only one with a defined structure. Prokes *et al.* first showed the direct connection of the visible PL in aged PS with oxygen TDs and linked them to NBOHCs.[54] NBOHCs have been observed in silica fibers irradiated by various rays, and they have various types with different PL efficiency and PL peak position.[54,55] In our nc-Si/SiO₂ film, based on the following arguments, it is more proper to use oxygen TD-like defect states to describe the visible PL features. (1) The observation of visible PL is dependent on the existence of crystalline Si, whereas the existence of NBOHCs does not depend on that of crystalline silicon. (2) The visible PL can be adjusted from 1.3 to 1.75 eV in our case. This range is much larger than the spectral range of visible PL from NBOHCs. (3) The observed spectral change can be well explained using the formation and decay kinetics of oxygen TDs. Since the studies of oxygen TDs have only been restricted to bulk crystalline Si, the effects of nc-Si dimension and interfacial environment around nc-Si on oxygen TDs have not been involved. However we can imagine that in nc-Si/SiO₂ system the formation and decay, the structure of oxygen TDs are much more complex due to the distribution of nc-Si size and that of the interfacial environment.[32] Up to now, since the consensus about the

structure and composition of oxygen TDs in bulk crystalline Si has not been reached, we will not speculate on the possible structure of oxygen TDs in the nc-Si systems here.

Based on the obtained results, the core structure for Si–O related surface species in different systems should be similar and include Si–O bonds. The core structure provides the common features: the visible PL with microsecond lifetimes at room temperature. The detailed structure, however, can be different due to variances in the microenvironment around nc-Si by different preparations. This can explain differences of visible PL, such as the distribution of the peak energies from 1.5 to 2.1 eV observed from different systems and the different dependence of visible PL on preparation conditions (here, the unique dependence of the visible PL on annealing conditions in our system).

One interesting phenomenon is that the PL decay times for Si=O surface states by the measurement of Wolkin *et al.* are in the microsecond range at room temperature, similar to those of PS itself.[15] Wang *et al.*[18] showed that the decay times of the bleach band at 1235 cm⁻¹ (Si–O stretching vibration) in PS are similar to the observed decay times of the visible PL in the same sample. The confusion and debate with regards to the origin of visible PL may somehow relate to this overlap of both peak energies and lifetimes.

V. CONCLUSIONS

The main conclusions are summarized as follows:

(1) The visible PL originates from oxygen TD-like defect states (Si NL8 and Si NL10 centers), which are created during FG annealing.

(2) The oscillatory behavior observed between 1.75 and 1.5 eV upon annealing at 400 °C can be explained by the variance in the growth and decay kinetics of Si NL8 and Si NL10 centers. Since it is a pure kinetic one, this excludes the possibilities of the structural phase transition or the size variation of nc-Si itself as the oscillatory element.

(3) Due to the easy control of the annealing condition, the visible PL can be finely tuned between 1.3 and 1.75 eV. The PL intensity shows a maximum around 1.5 ± 0.05 eV. The spectral shift from 1.3 to 1.55 eV is connected with both the QSE and the formation and decay kinetics of oxygen TD-like defect states while the spectral shift between 1.55 and 1.75 eV is mainly connected with the variation in concentrations of two oxygen TD-like defect states upon annealing.

(4) The nc-Si not only contributes to the light excitation process, but the existence of nc-Si is a prerequisite for the formation of oxygen TD-like defect states as well. Since the visible PL comes from interfacial defect states, PLE spectra show no obvious dependence on emission wavelengths.

In summary, we reported some experimental results of the visible PL from nc-Si/SiO₂ films produced by plasma CVD and subsequent post-treatment. The visible PL shows a universal trend upon annealing conditions. This dependence of the visible PL on annealing conditions in this system has not been reported in PS or in other nc-Si systems. This indicates that apart from the common features of Si–O related visible PL, the detailed configuration and composition of this PL center by different synthesis methods may be different and possess some features of their own.

[1]L. T. Canham, Appl. Phys. Lett. **57**, 1046 (1990).

[2]Y. Kanemitsu, Phys. Rep. **263**, 1 (1995).

[3]A. G. Cullis, L. T. Canham, and P. D. J. Calcott, J. Appl. Phys. **82**, 909 (1997).

[4]P. D. G. Calcot, K. J. Nash, L. T. Canham, M. J. Kane, and D. Brumhead, J. Phys.: Condens. Matter **5**, L91 (1993).

[5]P. D. G. Calcot, K. J. Nash, L. T. Canham, M. J. Kane, and D. Brumhead, J. Lumin. **57**, 257 (1993).

[6]K. J. Nash, P. D. J. Calcott, L. T. Canham, and R. J. Needs, Phys. Rev. B **51**, 17698 (1995).

[7]A. Bsiesy *et al.*, Surf. Sci. **254**, 195 (1991).

[8]S. M. Brant, D. H. Fuchs, M. Stutzmann, J. Weber, and M. Cardona, Solid State Commun. **81**, 307 (1992).

[9]S. M. Prokes, J. U. Glembocki, U. M. Bermudez, R. Kaplan, E. L. Friedersdorf, and C. P. Searon, Phys. Rev. B **45**, 13788 (1992).

[10]C. Tsai, H. K. Li, S. D. Kinosky, Z. R. Qian, C. T. Hsu, T. J. Irby, S. K. Banerjee, K. B. Hance, and M. J. White, Appl. Phys. Lett. **60**, 1700 (1992).

[11]S. Veprek, M. Rückschloss, B. Landkammer, and O. Ambacher, Mater. Res. Soc. Symp. Proc. **298**, 117 (1993).

[12]F. Koch, V. Petrova-Koch, T. Muschik, and A. Nikolov, MRS Symposia Proceedings, Pittsburgh, PA, 1993, p 197.

[13]S. M. Prokes, Appl. Phys. Lett. **62**, 3244 (1993).

[14]L. J. Gole and A. D. Dixon, J. Phys. Chem. B **102**, 33 (1998); L. J. Gole, P. F. Dudel, D. Grantier, and A. D. Dixon, Phys. Rev. B **56**, 2137 (1997); J. L. Gole and D. A. Dixon, J. Phys. Chem. B **101**, 8098 (1997); J. L. Gole and A. D. Dixon, *ibid.* **102**, 1768 (1998).

[15]M. V. Wolkin, J. Jorne, P. M. Fauchet, G. Allan, and C. Delerue, Phys. Rev. Lett. **82**, 197 (1999).

[16]I. Coulthard, W. J. Antel, J. W. Freeland, T. K. Sham, S. J. Naftel, and P. Zhang, Appl. Phys. Lett. **77**, 498 (2000).

[17]H. E. Porteanu, E. Lifshitz, Th. Dittrich, and V. Petrova-Koch, Phys. Rev. B **60**, 15538 (1999).

[18]J. P. Wang, L. Song, B. S. Zou, and M. A. El-Sayed, Phys. Rev. B **59**, 5026 (1999).

[19]S. M. Prokes, J. Mater. Res. **11**, 305 (1996).

[20]F. Koch, V. Petrova-Koch, and T. Muschik, J. Lumin. **57**, 271 (1993).

[21]H. Takagi, M. Mitome, R. Yano, and T. Nakagi, Solid State Phys. **27**, 875 (1991).

[22]Y. Kanemitsu, T. Ogawa, K. Shiraishi, and K. Takeda, Phys. Rev. B **48**, 4883 (1993).

[23]Y. Maeda, N. Tsukamoto, Y. Yazawa, Y. Kanemitsu, and Y. Masumoto, Appl. Phys. Lett. **59**, 3168 (1991).

[24]M. H. Ludwig, E. E. Hummel, and M. Stora, Thin Solid Films **255**, 103 (1995).

[25]M. Rückschloss, B. Landkammer, O. Ambacher, and S. Veprek, J. Lumin. **57**, 1 (1993); M. Rückschloss, B. Landkammer, and S. Veprek, Appl. Phys. Lett. **63**, 11 (1993); M. Rückschloss, B. Landkammer, O. Ambacher, and S. Veprek, Mater. Res. Soc. Symp. Proc. **283**, 65 (1993); S. Veprek, T. Wirshiem, M. Rückschloss, Ch. Ossadnik, J. Dian, S. Perna, and I. Gregora, *ibid.* **405**, 141 (1996).

[26]S. Schuppler *et al.*, Phys. Rev. Lett. **72**, 2648 (1994).

[27]H. Mizuno, H. Koyama, and N. Koshida, Appl. Phys. Lett. **69**, 3779 (1996).

[28]H. Takagi, H. Ogawa, Y. Yamazaki, A. Ishizaki, and T. Nakagiri, Appl. Phys. Lett. **24**, 2379 (1990).

[29]T. Ito, T. Ohta, and A. Hiraki, Jpn. J. Appl. Phys., Part 2 **31**, L1 (1992).

[30]M. L. Brongersma, A. Polman, K. S. Min, E. Boer, T. Tambo, and H. A. Atwater, Appl. Phys. Lett. **72**, 2577 (1998).

[31]S. Veprek and T. Wirschem, *Handbook of Optical Properties* (Chemical Rubber Corp., Boca Raton, FL, 1997), p. 129.

[32]S. M. Prokes, W. E. Carlos, S. Veprek, and Ch. Ossadnik, Phys. Rev. B **58**, 15632 (1999).

[33]X. C. Wu, A. Bek, A. Bittner, K. Kern, Ch. Ossadnik, Ch. Eggs, and S. Veprek (unpublished).

[34]S. Veprek, Z. Iqbal, and F. A. Sarott, Philos. Mag. B **45**, 137 (1982).

[35]M. Konuma, H. Curtins, F. A. Sarott, and S. Veprek, Philos. Mag. B **55**, 377 (1987).

[36]Y. Kanemitsu, T. Futagi, T. Matsumoto, and H. Mimura, Phys. Rev. B **49**, 14732 (1994).

[37]R. E. Hummel, M. Ludwig, S. S. Chang, and G. LaTorre, Thin Solid Films **255**, 219 (1995).

[38]D. B. Mawhinney, J. A. Glass, Jr., and J. T. Yates, J. Phys. Chem. B **101**, 1202 (1997).

[39]B. Delly and E. F. Steigmeier, Appl. Phys. Lett. **67**, 2370 (1995).

[40]B. Delly and E. F. Steigmeier, Phys. Rev. B **47**, 1397 (1993).

[41]M. S. Hybertsen, Phys. Rev. Lett. **72**, 1514 (1994).

[42]T. Takagahara and K. Takeda, Phys. Rev. B **46**, 15578 (1992).

[43]C. Delerue, G. Allan, and M. Lannoo, Phys. Rev. B **48**, 11024 (1993).

[44]X. C. Wu, A. M. Bittner, K. Kern, Ch. Eggs, and S. Veprek, Appl. Phys. Lett. **77**, 645 (2000).

[45]H. Y. Xie, L. W. Wilson, M. F. Ross, A. J. Mucha, A. E. Fitzgerald, M. J. Macaulay, and D. T. Harris, J. Appl. Phys. **71**, 2403 (1992).

[46]N. Ookubo, J. Appl. Phys. **74**, 6375 (1993).

[47]P. V. Bondarenko, E. V. Borisenko, M. A. Dorofeev, N. I. Germanenko, and V. S. Gaponenko, J. Appl. Phys. **75**, 2727 (1994).

[48]S. Sinha, S. Banerjee, and M. B. Arora, Phys. Rev. B **49**, 5706 (1994).

[49]A. Kux and M. Ben Chorin, Phys. Rev. B **51**, 17535 (1995).

[50]K. O. Andersen and E. Veje, Phys. Rev. B **53**, 15643 (1996).

[51]T. Gregorkiewicz, H. H. P. Th. Bekman, and C. A. J. Ammerlaan, Phys. Rev. B **41**, 12628 (1990).

[52]T. Gregorkiewicz, D. A. van Wezep, H. H. P. Th. Bekman, and C. A. J. Ammerlaan, Phys. Rev. B **35**, 3810 (1987).

[53]J. Michel and C. L. Kimerling, *Semiconductors and Semimetals* (Academic, New York, 1984), Vol. 42, p. 251.

[54]S. M. Prokes and O. J. Glembocki, Phys. Rev. B **49**, 2238 (1994); S. M. Prokes, W. E. Carlos, and O. J. Glembocki, *ibid.* **50**, 17093 (1994).

[55]S. Munekuni, T. Yamanaka, Y. Shimogaichi, R. Tohmon, Y. Ohni, K. Nagasawa, and Y. Hama, J. Appl. Phys. **68**, 1212 (1990).